SUPPORTING INFORMATION

Molecular crowding overcomes destabilizing mutations in a bacterial ribozyme

Hui-Ting Lee, Duncan Kilburn, Reza Behrouzi, Robert M. Briber, and Sarah A. Woodson

Supplementary Methods

Identification of folding intermediates by native PAGE.

The ribozyme conformations separated by native polyacrylamide electrophoresis (PAGE) were identified by comparison with SAXS data and by comparison of the electrophoretic mobility of WT and mutant ribozymes. The native PAGE mobility of all ribozymes incubated at 0 and 15 mM $MgCl_2$ is shown in Figure S1. The WT RNA forms two major bands when pre-folded without Mg^{2+} (1). The population of the fastest migrating band increases with increasing $MgCl_2$ concentration, and was assigned to the folded species (I_C+N). The band with intermediate mobility decreases in intensity with $MgCl_2$ concentration, and was assumed to arise from the unfolded species in solution, U. The change in the populations of these two bands coincides with the main folding transition in SAXS titration curves (see below and Fig. S3a), corroborating these assignments. Because the *Azoarcus* ribozyme folds rapidly, a portion of the unfolded RNA also reaches the folded state as the sample is loaded into the gel containing 3 mM $MgCl_2$, as illustrated in Fig. S1c. As a result, some of the RNA appeared to be folded even when the sample was prepared without $MgCl_2$.

The WT ribozyme forms a third minor band with slow PAGE mobility. This slow-moving conformer was much stronger in the L9 mutant ribozyme and was assigned to the extended intermediate (I_U) that is highly populated in SAXS data on the L9 mutant. The correspondence between folding intermediates detected by native PAGE and by SAXS for the remaining mutants confirm this assignment of the U and I_U states (Fig. S3).

An analysis of the full scattering curves indicated that the unfolded ribozyme in low Mg^{2+} behaves as a stiff rod, while the I_U ensemble is closer to a relaxed coil (2,3). This may explain why the rod-like U state travels faster through the gel than the I_U relaxed coil, even though the U ensemble has a larger R_g than the I_U ensemble according to solution scattering experiments. We note that the U and I_U structures can collapse into a more folded conformation in the gel running buffer, and thus their conformation in the gel may not be the same as in solution. Finally, rapid chemical exchange between different conformers during electrophoresis may contribute to the observed mobility of certain mutant RNAs (4).

The mutants in Figure S1 can be classified into three groups based on the distribution and mobility of bands in high salt: (1) P6 (A97U), J2/3 (A39U) and TH migrate as a single band that travels slightly slower than the WT N+I_C band; (2) L2, L2P6 and L2TH form a single band with a mobility similar to that of the WT U band; and (3) L9, L2L9, L9P6, L9TH and L2THL9 form two folded species that always had the same response to $MgCl_2$ and so were quantified together

as two alternative forms of N or I_C. The mobility of the unfolded ribozyme in no Mg^{2+} followed the same classification as the folded RNA. Ribozymes carrying J2/3 and P6 point mutations were not used for the experiments in this work but are discussed elsewhere (5).

Populations of folding intermediates from SAXS and native PAGE.

We calculated the molar fraction of the three species, U, I_U and I_C, using parameters from fits of SAXS titration curves to a three-state partition function (6):

$$\text{U:}\quad f_U(C) = \frac{1}{1+\left(C/C_{m1}\right)^{n1}+\left(C/C_{m2}\right)^{n2}} \qquad \text{(Eq. S1)}$$

$$\text{I}_\text{U}\text{:}\quad f_{IU}(C) = \frac{\left(C/C_{m1}\right)^{n1}}{1+\left(C/C_{m1}\right)^{n1}+\left(C/C_{m2}\right)^{n2}} \qquad \text{(Eq. S2)}$$

$$\text{I}_\text{C}\text{:}\quad f_{IC}(C) = \frac{\left(C/C_{m2}\right)^{n2}}{1+\left(C/C_{m1}\right)^{n1}+\left(C/C_{m2}\right)^{n2}} \qquad \text{(Eq. S3)}$$

Each term $(C/C_m)^n$ describes the statistical weight of the U, I_U and I_C states at Mg^{2+} concentration C, and was obtained assuming that the observed $R_g^2 = \Sigma_i\ \chi_i(R_{g,i})^2$ (6). The same analysis can also be applied to other mutants (Fig. S3 a,c-f). The resulting populations diagram how a crowded environment changes the folding intermediates of the mutant ribozymes, but without substantially changing the propensity of a given ribozyme sequence to form the extended I_U state or other non-native states.

The same three-state model was used to fit the data from native PAGE. To account for the redistribution of the U state into folded and "unfolded" conformations in the gel, the slow I_U and fast I_C + N bands were assumed to originate from a combination of U and I_U or U and I_C in solution (Fig. S1c). The fraction of counts in each band of the gel were fit as in Eq. S3, setting $f_{slow} = f(U+I_U)$, $f_{int} = fU$, and $f_{fast} = f(U+I_C)$.

Analysis of single turnover ribozyme activity assays

Cleavage of the RNA substrate under single-turnover conditions (~1000-fold enzyme excess over substrate) resulted in a burst of product within the first 25 s at high Mg^{2+} concentration, in which all of the ribozyme has folded. By contrast, progress curves at low Mg^{2+} displayed biphasic or compressed exponential (lag) kinetics (Fig. S4), indicating the ribozyme-substrate complex must undergo one or more slower steps during the reaction (7). The fraction of product over time was fit to

$$f(t) = A\left[1-\exp\left(-k_1 t\right)^{\beta}\right] - \left(0.5-A\right)\left[1-\exp\left(-k_2 t\right)\right] \qquad \text{(Eq. S4)}$$

in which t is time, A is the amplitude and k_1 is the observed rate constant of the initial phase, β is the stretching parameter and k_2 is the rate constant of the slow (minor) phase.

Conformational changes that limit the observed cleavage rate could include reorganization of the guanosine binding site or docking of the P1 helix which is less favorable in the *Azoarcus*

ribozyme than in the *Tetrahymen*a group ribozyme (8). Conformational changes requiring several minutes could include refolding of the ribozyme tertiary structure. The addition of 18% PEG reduces the initial rate of the first turnover, k_1, which can be accounted for by the increased viscosity of the solution (2). This is likely not due to slower binding of the RNA substrate, as native gel mobility shift experiments showed that the RNA substrate binds in less than 25 s under all conditions tested here, see Figure S5.

Because conformational changes leading to the native state are slower than the rate of chemistry (9), the yield of product in the initial burst should correspond to the fraction native ribozyme, under our single-turnover conditions. Native gel mobility shift assays confirmed that the RNA substrate is bound within the shortest time of our assay (Fig. S5). The amount of product formed in the first 13 or 25 s versus $MgCl_2$ concentration (Fig. S7) yielded a cooperative folding transition that can be fit to a two-state model as previously described (5), with midpoints of 2.5 ± 0.11 mM and 2.86 ± 0.17 mM $MgCl_2$, for the WT and TH ribozymes, respectively. These values are consistent with values previously reported for the WT and TH ribozymes after 20 s of reaction (5).

The steepness and midpoint of the apparent folding transition to the native state depends on the time allowed for the ribozyme to react (Fig. S7). The amount of product formed within the first 25 s was taken to represent the fraction of ribozymes that was immediately active upon the

addition of substrate. Comparing the titration curves for different reaction times revealed that most of the reactions completed the initial phase (*A* in eq. S4) after 3 min (black data in Fig. S7). Therefore, the amount of product formed within 3 min was taken to represent the total fraction of "refoldable" ribozyme competent to attain the active structure (7).

Table S1: Thermodynamic parameters obtained from SAXS

RNA	$[Mg^{2+}]_{½}$ (mM)	*n*	ΔG_{37} (kcal/mol)	$\Delta\Delta G_{37}$ (kcal/mol)	$\Delta\Delta\Delta G_{37}$ (kcal/mol)
WT	0.47 ± 0.02	5.25 ± 0.81	0.00 ± 0.11		
WT+18%PEG	0.28 ± 0.00	5.52 ± 0.16	-1.77 ± 0.05		
L2	0.53 ± 0.01	5.77 ± 0.58	0.45 ± 0.11	0.45 ± 0.16	
L2+18%PEG	0.25 ± 0.01	5.24 ± 0.38	-2.06 ± 0.13	-0.29 ± 0.14	-0.74 ± 0.21
TH	0.56 ± 0.01	7.68 ± 0.48	0.83 ± 0.08	0.83 ± 0.14	
TH+18%PEG	0.27 ± 0.01	6.32 ± 0.42	-2.13 ± 0.13	-0.36 ± 0.14	-1.19 ± 0.20
L9	0.62 ± 0.01	4.40 ± 0.33	0.74 ± 0.09	0.74 ± 0.14	
L9+18%PEG	0.35 ± 0.01	6.36 ± 0.35	-1.16 ± 0.07	0.61 ± 0.09	-0.13 ± 0.17
L2/TH	0.47 ± 0.01	6.15 ± 0.52	0.00 ± 0.08	0.00 ± 0.14	
L2/TH+18%PEG	0.24 ± 0.01	5.58 ± 0.59	-2.26 ± 0.21	-0.49 ± 0.22	-0.49 ± 0.26
L2/L9	0.64 ± 0.01	4.40 ± 0.56	0.83 ± 0.16	0.83 ± 0.20	
L2/L9+18%PEG	0.34 ± 0.01	4.59 ± 0.42	-0.91 ± 0.08	0.86 ± 0.10	0.03 ± 0.22
TH/L9	0.56 ± 0.02	4.34 ± 0.44	0.46 ± 0.12	0.46 ± 0.16	
TH/L9+18%PEG	0.28 ± 0.01	5.23 ± 0.33	-1.62 ± 0.08	0.16 ± 0.10	-0.3 ± 0.19
L2/TH/L9	0.65 ± 0.01	4.61 ± 0.58	0.94 ± 0.16	0.94 ± 0.20	
L2/TH/L9+18%PEG	0.33 ± 0.01	5.86 ± 0.56	-1.24 ± 0.12	0.53 ± 0.13	-0.41 ± 0.24

All the experiments were done with 0.4 mg/mL RNA in 20 mM Tris-HCl, pH 7.5 at 37 °C. Parameters for I_U to I_C transition were obtained from the change in R_g^2 vs. $[Mg^{2+}]$ (see Methods). ΔG(37 °C) in kcal/mol was evaluated at $[Mg^{2+}] = [Mg^{2+}]_{1/2}^{WT} = 0.47$ mM in dilute buffer; note that ΔG is evaluated relative to $[Mg^{2+}]_{1/2}^{WT}$ in each solution condition in Fig. 5. The energy perturbation due to the mutation is $\Delta\Delta G = \Delta G^{mut} - \Delta G^{WT}$; $\Delta\Delta\Delta G = \Delta\Delta G(PEG) - \Delta\Delta G(H_2O)$. Errors (± S.D.) were calculated from bootstrap residuals (see Methods).

Table S2: Thermodynamic parameters obtained from activity assays quenched at 25 s

RNA	$[Mg^{2+}]_{1/2}$ (mM)	*n*	ΔG_{37} (kcal/mol)	$\Delta\Delta G_{37}$ (kcal/mol)	$\Delta\Delta\Delta G_{37}$ (kcal/mol)
WT	1.56 ± 0.06	3.54 ± 0.32	0.00 ± 0.11		
WT+18%PEG	1.34 ± 0.07	2.57 ± 0.18	-0.24 ± 0.11		
L2	1.79 ± 0.06	3.32 ± 0.14	0.28 ± 0.08	0.28 ± 0.14	
L2+18%PEG	1.25 ± 0.08	3.26 ± 0.15	-0.44 ± 0.14	-0.20 ± 0.18	-0.48 ± 0.23
TH	1.96 ± 0.03	3.95 ± 0.15	0.55 ± 0.06	0.55 ± 0.13	
TH+18%PEG	1.18 ± 0.05	3.48 ± 0.20	-0.60 ± 0.09	-0.36 ± 0.14	-0.91 ± 0.19
L9	2.12 ± 0.05	5.71 ± 0.28	1.08 ± 0.11	1.08 ± 0.16	
L9+18%PEG	1.22 ± 0.02	4.85 ± 0.14	-0.73 ± 0.06	-0.49 ± 0.13	-1.57 ± 0.21
L2/TH	2.08 ± 0.04	5.38 ± 0.28	0.95 ± 0.09	0.95 ± 0.14	
L2/TH+18%PEG	1.25 ± 0.10	3.38 ± 0.20	-0.46 ± 0.10	-0.22 ± 0.14	-1.17 ± 0.20
L2/L9	2.85 ± 0.05	4.53 ± 0.14	1.68 ± 0.07	1.68 ± 0.13	
L2/L9+18%PEG	1.19 ± 0.03	6.19 ± 0.37	-1.03 ± 0.11	-0.79 ± 0.16	-2.47 ± 0.21
TH/L9	4.03 ± 0.34	2.49 ± 0.17	1.45 ± 0.18	1.45 ± 0.21	
TH/L9+18%PEG	1.40 ± 0.05	4.88 ± 0.34	-0.32 ± 0.12	-0.08 ± 0.16	-1.53 ± 0.26
L2/TH/L9	3.95 ± 0.09	3.86 ± 0.16	2.20 ± 0.11	2.20 ± 0.16	
L2/TH/L9+18%PEG	1.45 ± 0.05	6.40 ± 0.56	-0.30 ± 0.16	-0.06 ± 0.19	-2.26 ± 0.25

All the experiments were done with 0.4 mg/ml RNA and 20 mM Tris-HCl, pH 7.5 at 37 °C. ΔG was evaluated at 1.56 mM Mg^{2+} at 37 °C. See legend to Table S1 for definitions.

Table S3: Thermodynamic parameters obtained from activity assays quenched at 3 min.

RNA	$[Mg^{2+}]_{½}$ (mM)	*n*	ΔG_{37} (kcal/mol)	$\Delta\Delta G_{37}$ (kcal/mol)	$\Delta\Delta\Delta G_{37}$ (kcal/mol)
WT	0.88 ± 0.04	5.37 ± 0.88	-1.89 ± 0.40	±	
WT+18%PEG	0.63 ± 0.02	6.20 ± 0.48	-3.45 ± 0.22	±	
L2	0.98 ± 0.05	4.60 ± 0.35	-1.31 ± 0.19	0.57 ± 0.44	
L2+18%PEG	0.73 ± 0.02	8.45 ± 0.76	-3.94 ± 0.30	-0.49 ± 0.37	-1.06 ± 0.57
TH	1.38 ± 0.05	4.49 ± 0.32	-0.34 ± 0.11	1.55 ± 0.41	
TH+18%PEG	0.69 ± 0.02	7.11 ± 0.43	-3.56 ± 0.23	-0.11 ± 0.32	-1.66 ± 0.52
L9	1.34 ± 0.03	4.09 ± 0.50	-0.38 ± 0.06	1.51 ± 0.40	
L9+18%PEG	0.78 ± 0.05	8.76 ± 0.38	-3.73 ± 0.27	-0.28 ± 0.35	-1.79 ± 0.53
L2/TH	1.64 ± 0.06	4.62 ± 0.56	0.14 ± 0.12	2.03 ± 0.42	
L2/TH+18%PEG	0.79 ± 0.02	9.32 ± 0.41	-3.89 ± 0.21	-0.44 ± 0.31	-2.47 ± 0.52
L2/L9	1.81 ± 0.04	4.42 ± 0.34	0.40 ± 0.07	2.29 ± 0.40	
L2/L9+18%PEG	0.91 ± 0.01	8.71 ± 0.45	-2.88 ± 0.16	0.57 ± 0.27	-1.72 ± 0.48
TH/L9	2.64 ± 0.14	3.28 ± 0.40	1.06 ± 0.13	2.95 ± 0.42	
TH/L9+18%PEG	1.04 ± 0.02	6.69 ± 0.40	-1.67 ± 0.12	1.79 ± 0.26	-1.16 ± 0.49
L2/TH/L9	2.98 ± 0.14	3.48 ± 0.38	1.38 ± 0.14	3.27 ± 0.42	
L2/TH/L9+18%PEG	1.13 ± 0.03	7.29 ± 0.90	-1.44 ± 0.11	2.01 ± 0.25	-1.26 ± 0.49

All the experiments were done with 0.4 mg/ml RNA and 20 mM Tris-HCl, pH 7.5 at 37 °C. ΔG was evaluated at 1.56 mM Mg^{2+} as in Table S2. See the legend to Table S1 for definitions.

Figure S1

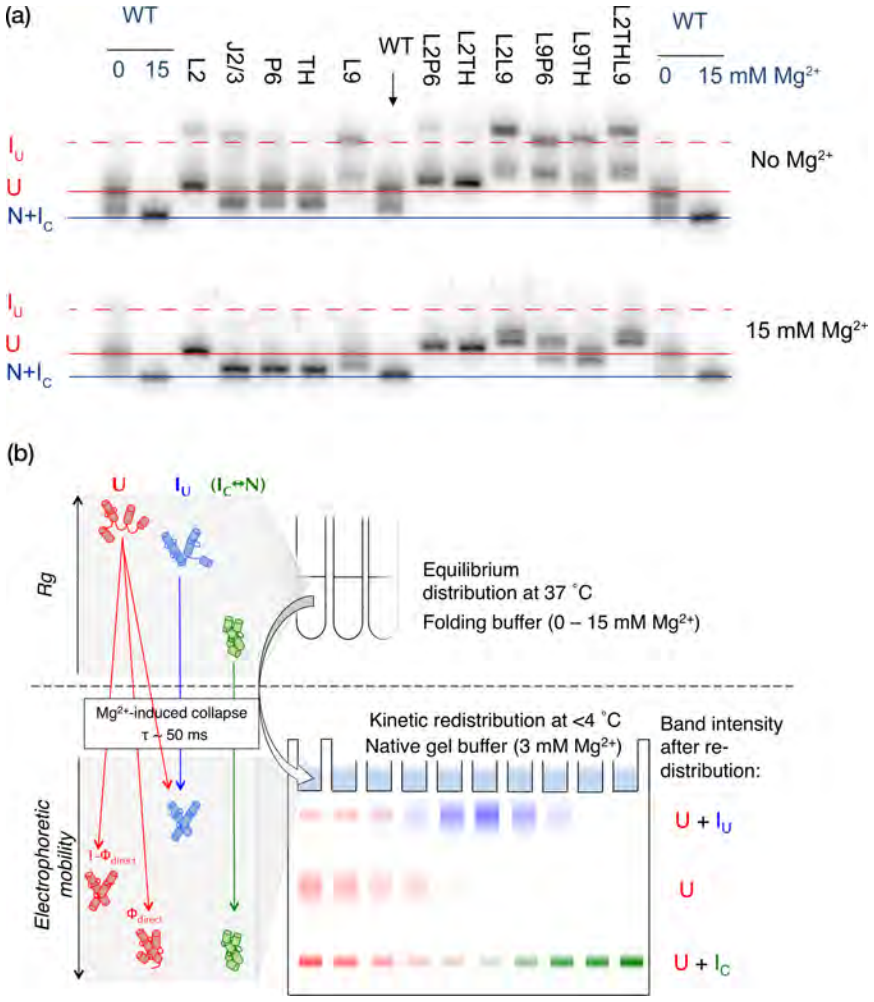

Figure S1. Native gel mobility of the *Azoarcus* L-9 ribozyme. a. Wild type and mutant ribozyme RNA was pre-folded at 20 mM Tris-HCl, pH 7.5, without $MgCl_2$ (top) or with 15 mM $MgCl_2$ (bottom). The gel running buffer has 20 mM Tris-HCl, pH 7.5, 3 mM $MgCl_2$. WT 0 and 15 indicate unfolded and folded WT controls. Lines mark the electrophoretic mobility of WT conformers: blue, I_C and N; solid red, U; and dashed red, I_U. Ribozymes carrying J2/3 and P6 point mutations were not used in the other experiments in this work. **b.** Scheme depicting the redistribution of the unfolded RNA into slow, intermediate and fast migrating conformations as RNA samples are loaded into the gel.

Figure S2

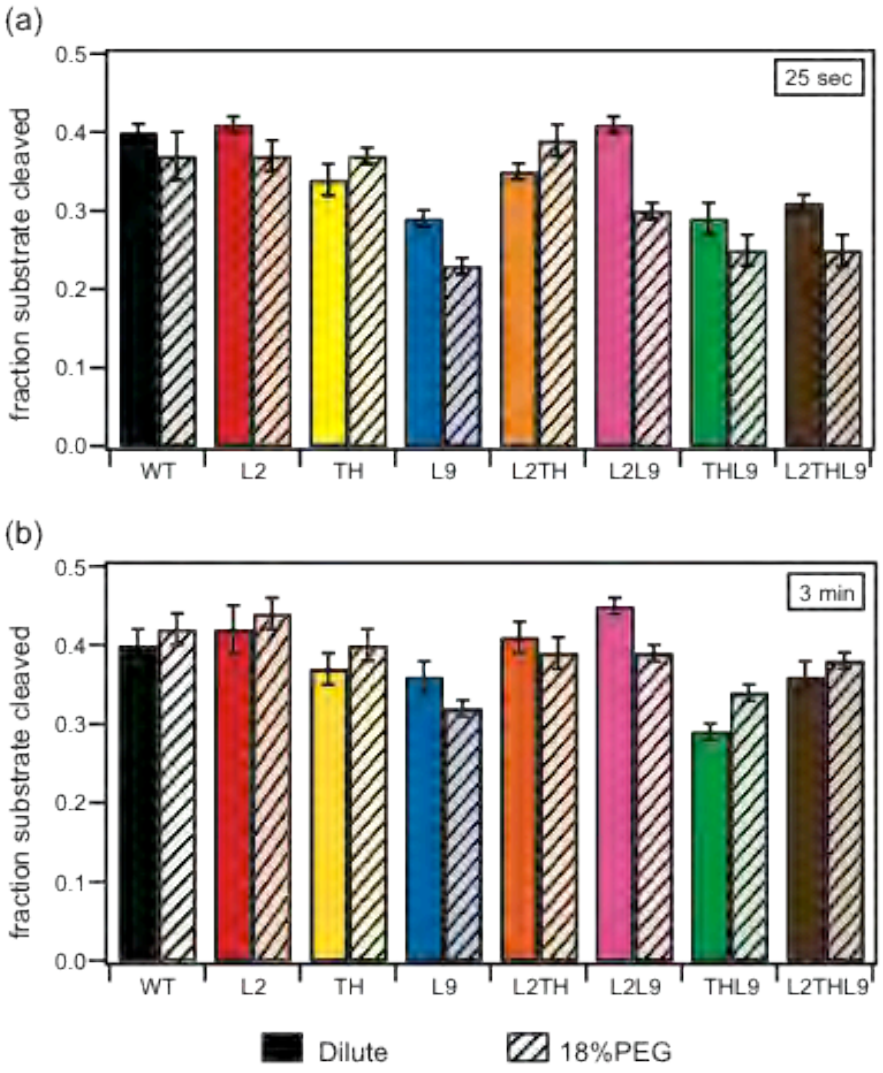

Figure S2. Maximum activity of each ribozyme in dilute solution (solid bars) and 18% PEG (stripes). The maximum activity was measured at 15 mM $MgCl_2$ in dilute solution and 5 mM $MgCl_2$ in 18% PEG.

Figure S3

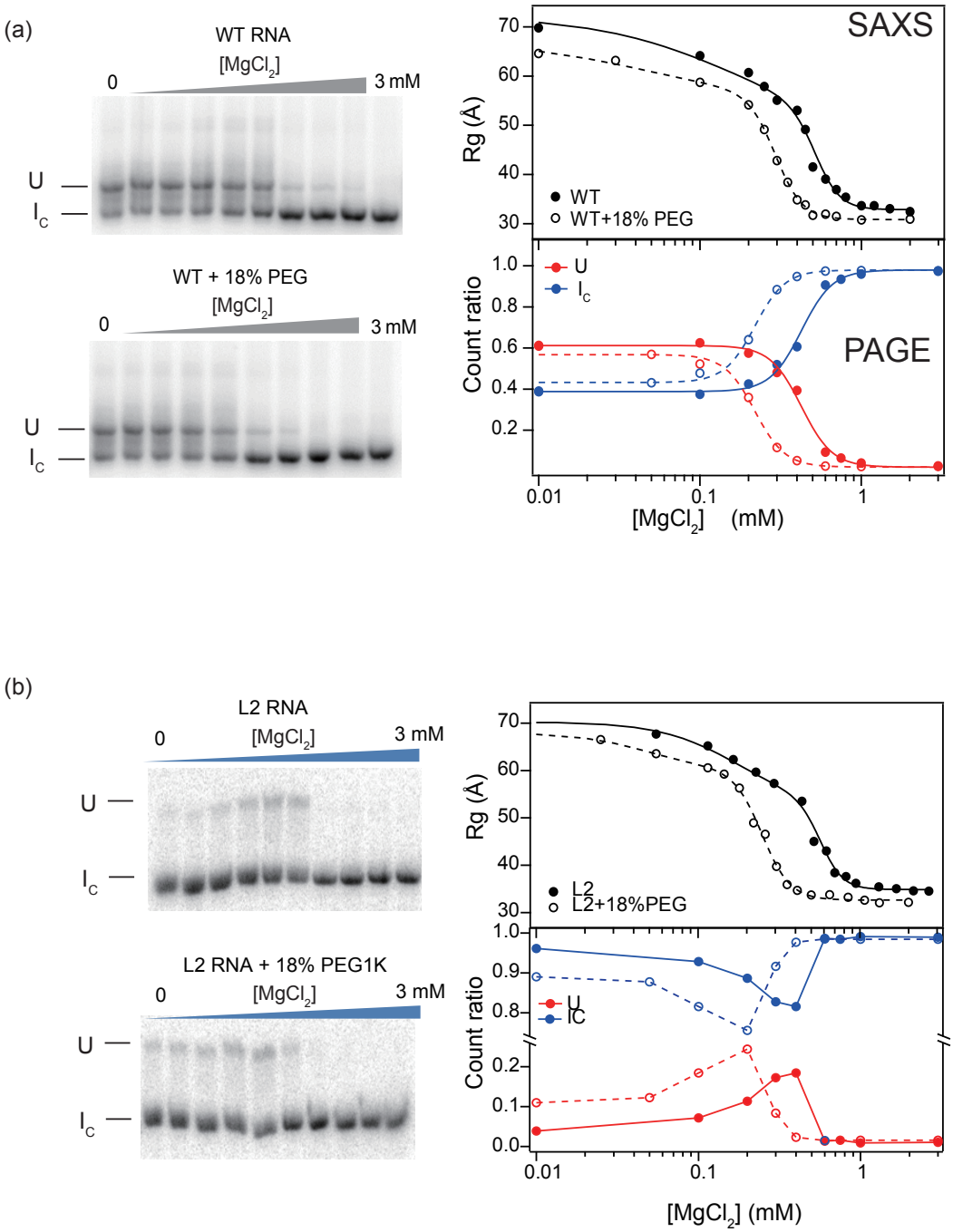
(a)
WT RNA
[MgCl2]
0
3 mM
U
IC
WT + 18% PEG
[MgCl2]
0
3 mM
U
IC
SAXS
Rg (Å)
WT
WT+18% PEG
Count ratio
U
IC
PAGE
[MgCl2] (mM)
(b)
L2 RNA
[MgCl2]
0
3 mM
U
IC
L2 RNA + 18% PEG1K
[MgCl2]
0
3 mM
U
IC
Rg (Å)
L2
L2+18%PEG
Count ratio
U
IC
[MgCl2] (mM)

Figure S3 cont.

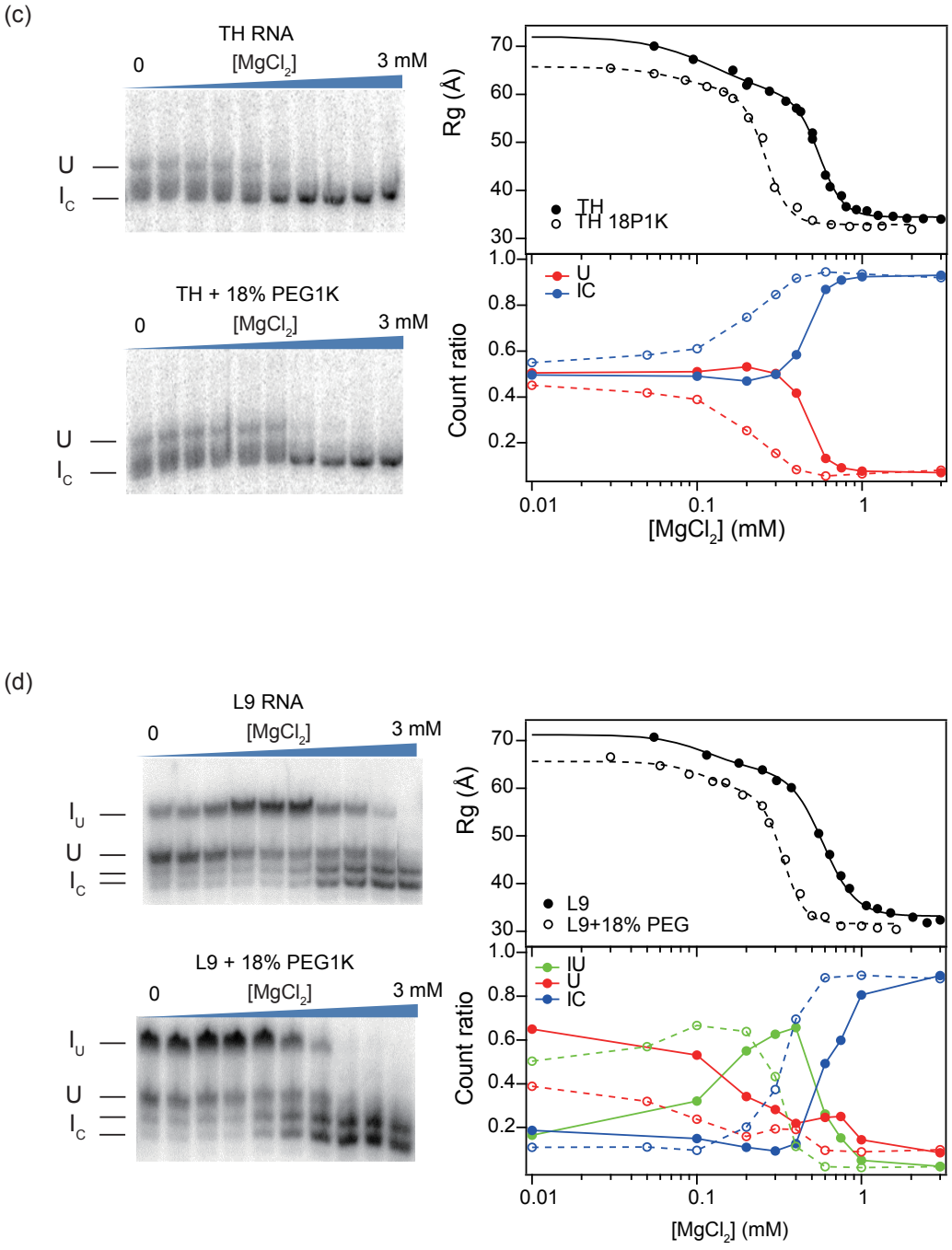

Figure S3 cont.

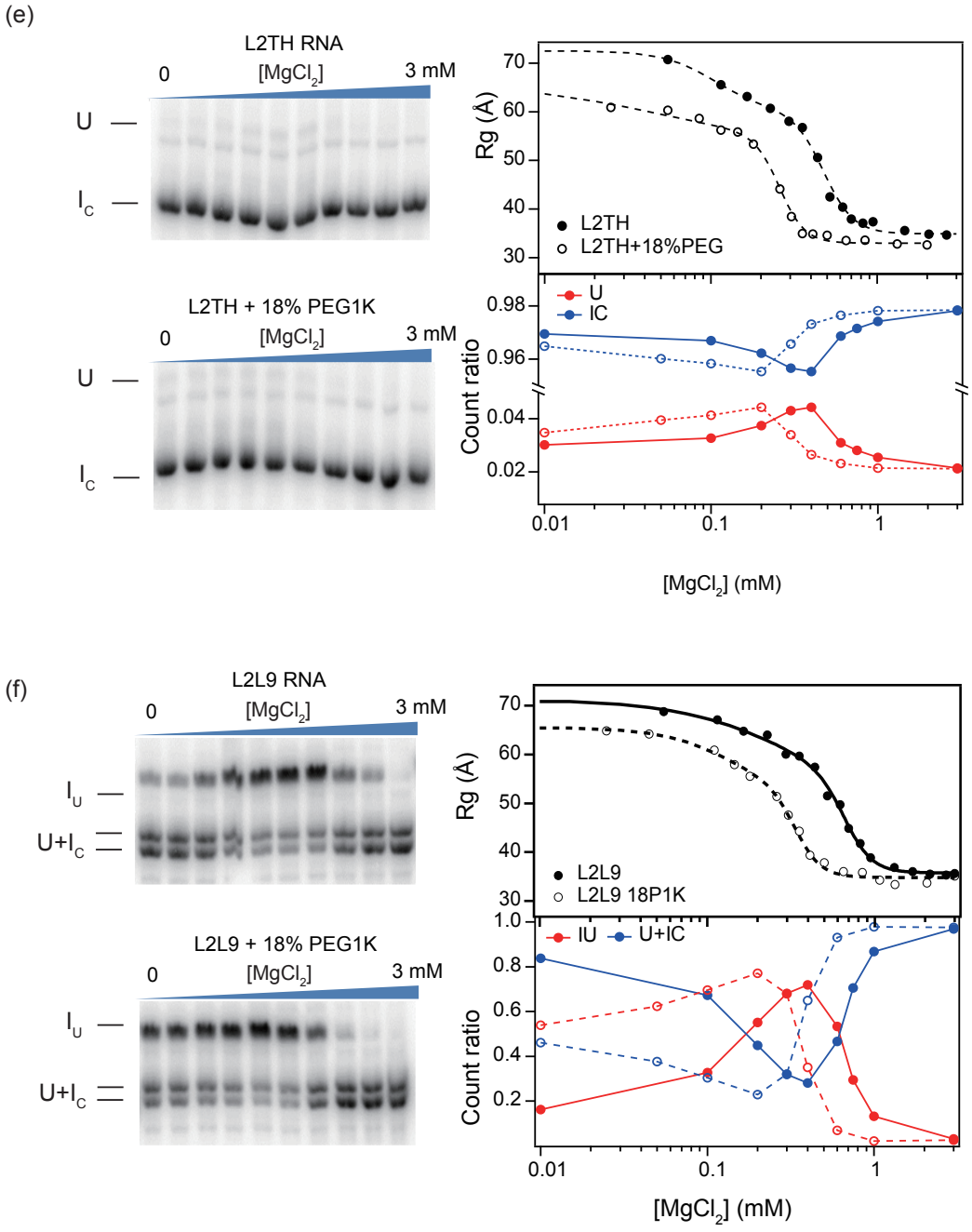

Figure S3 cont.

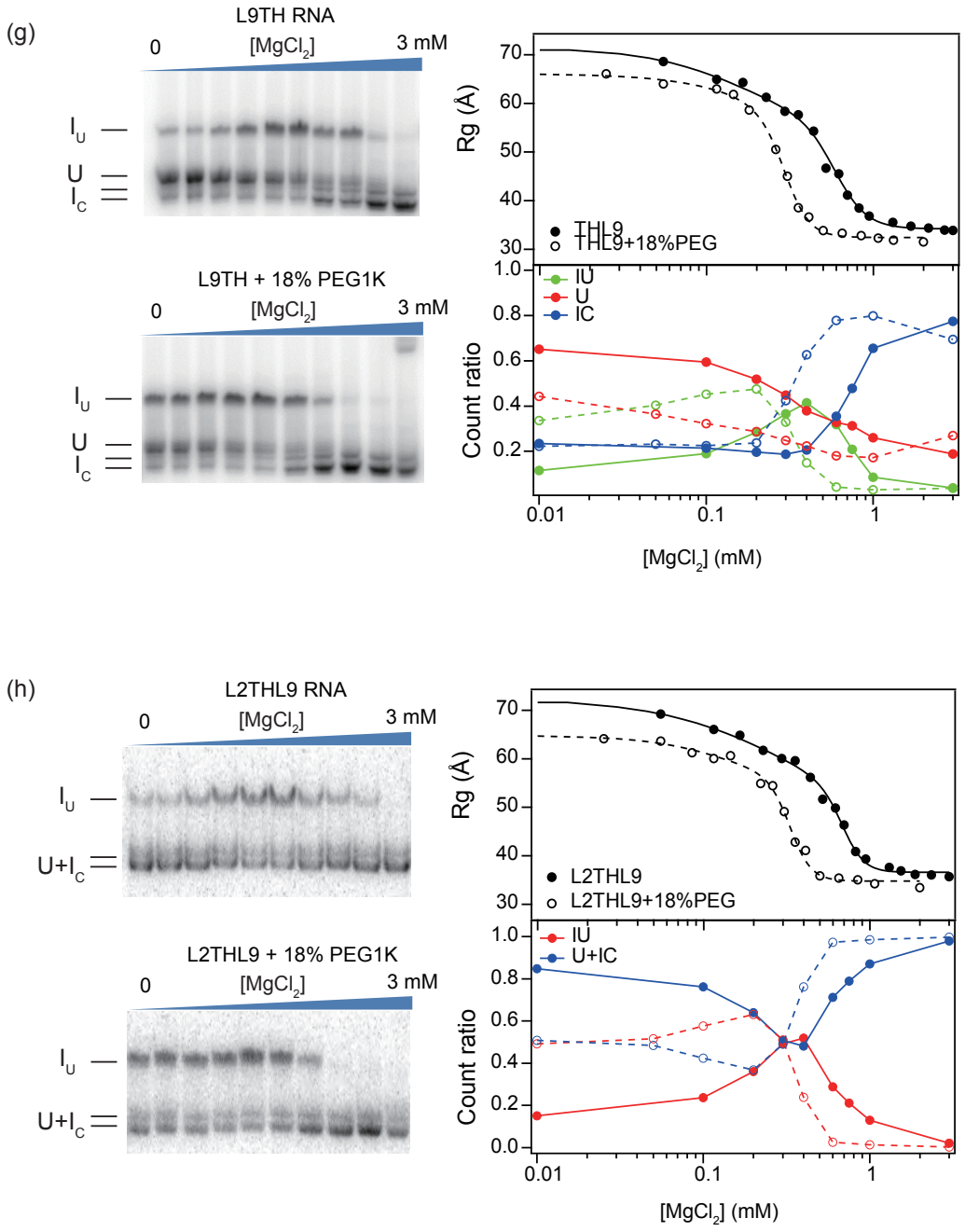

Figure S3. Comparison of RNA folding by native gel and SAXS. Compaction and folding of the *Azoarcus* ribozyme was measured by native 8% PAGE and SAXS under the same conditions (see Methods). Left, native gels comparing RNA folded in dilute buffer or in 18% PEG. Right, R_g or the fraction folded RNA (I_C) vs. [$MgCl_2$]. The SAXS data were fit with a 3-state folding model (lines), whereas the observed fraction of counts in each band of the native gel were interpolated

by a smooth curve. The two bands with fastest mobility in L9, L2L9, THL9, and L2THL9 were considered together as the compact intermediate.

Figure S4

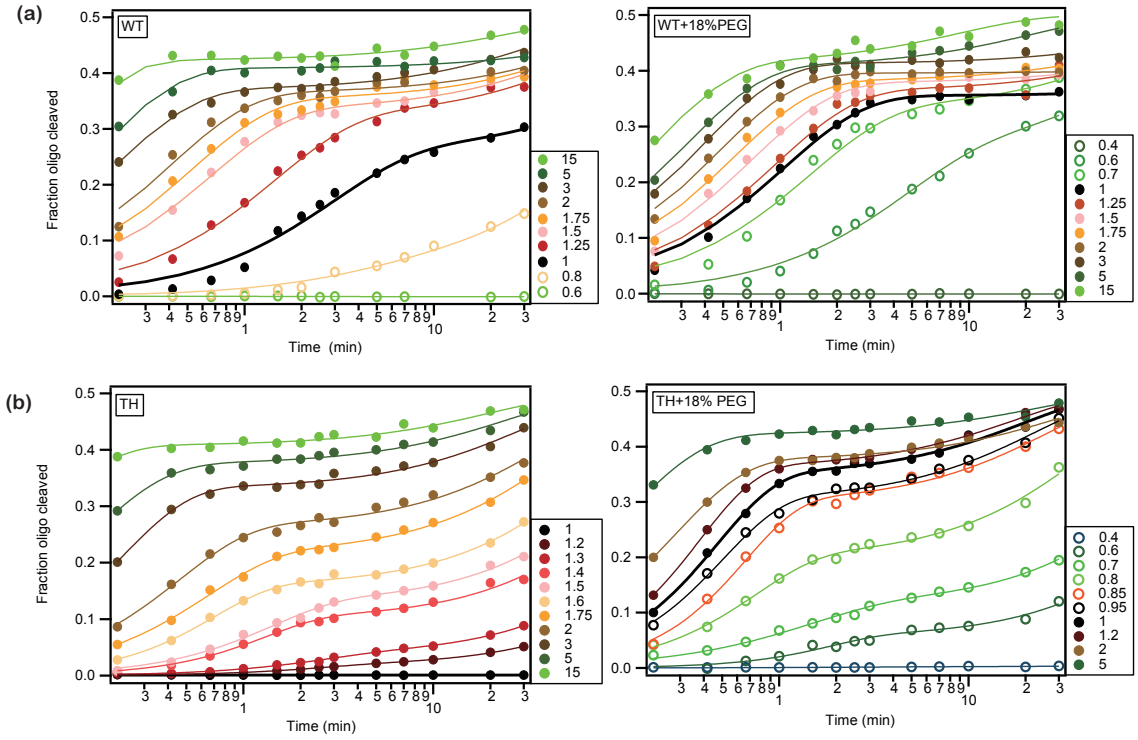

Figure S4. Substrate cleavage as a function of time in different [$MgCl_2$]. All the experiments were done with 0.4 mg/ml L-3 ribozyme and 20 mM Tris-HCl, pH 7.5, at 37 °C. Progress curves were fit to compressed exponential rate equation (eq. S4). Colors indicate the same [$MgCl_2$] in each plot. (a), WT ribozyme in dilute buffer; (b) WT ribozyme in 18% PEG; (c) TH ribozyme in dilute buffer; (d) TH ribozyme in 18% PEG.

Figure S5

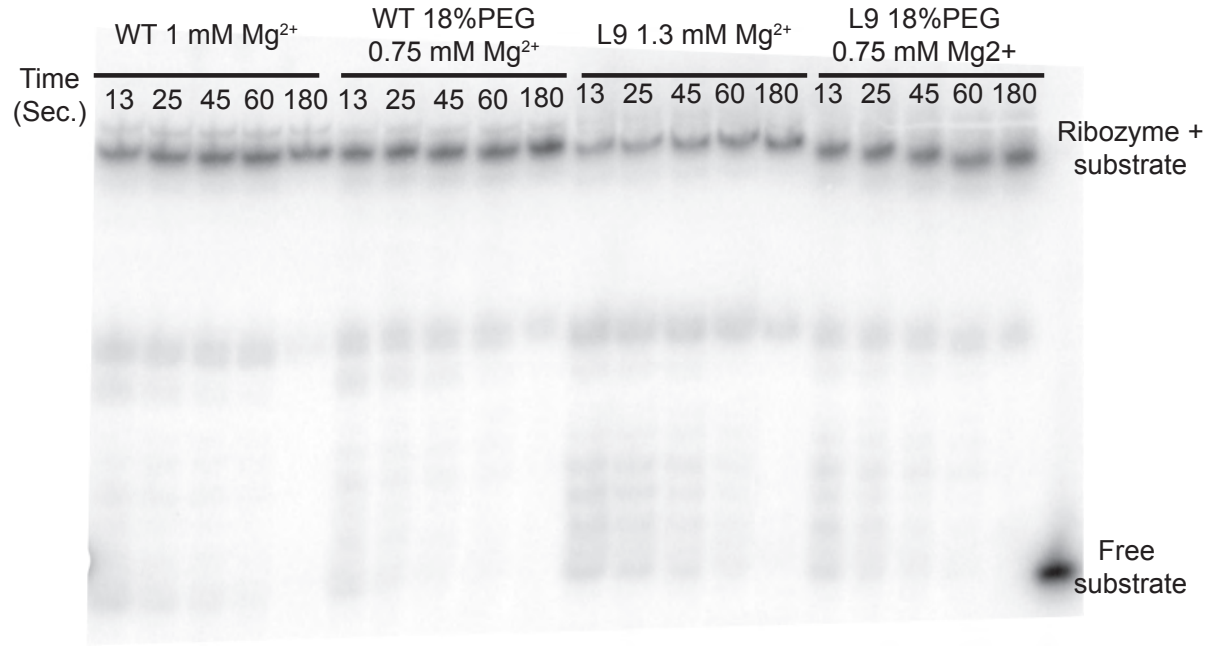

Figure S5. Binding of substrate. ~10 nM ^{32}P-labeled substrate RNA was mixed with 0.4 mg/ml L-3 ribozyme and 20 mM Tris-HCl, pH 7.5, at 37 °C for 13-180 s before samples were loaded. The gel running buffer contains 20 mM Tris-HCl, pH 7.5, 3 mM $MgCl_2$.

Figure S6

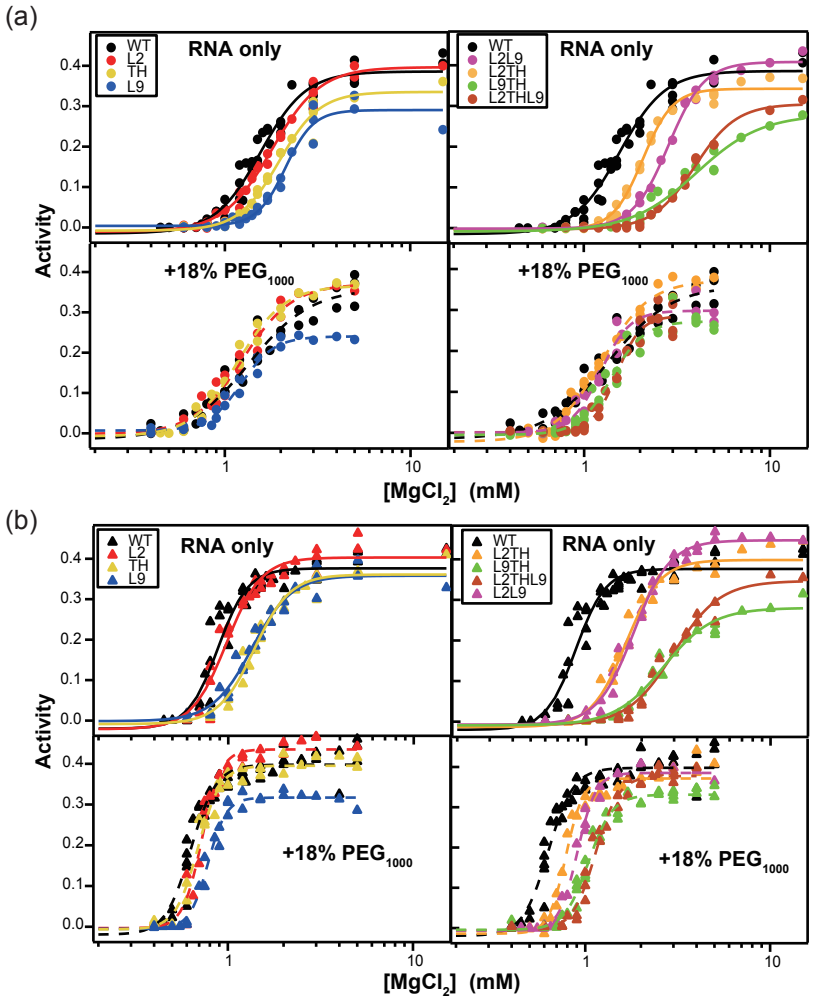

Figure S6. Activity of each mutant as a function of $MgCl_2$ concentration. All the substrate cleavage experiments were done with 0.4 mg/ml ribozyme and 20 mM Tris-HCl, pH 7.5, at 37 °C. Fraction of ribozyme•substrate complexes that formed product after (a) 25 s and (b) 3 min.

Figure S7

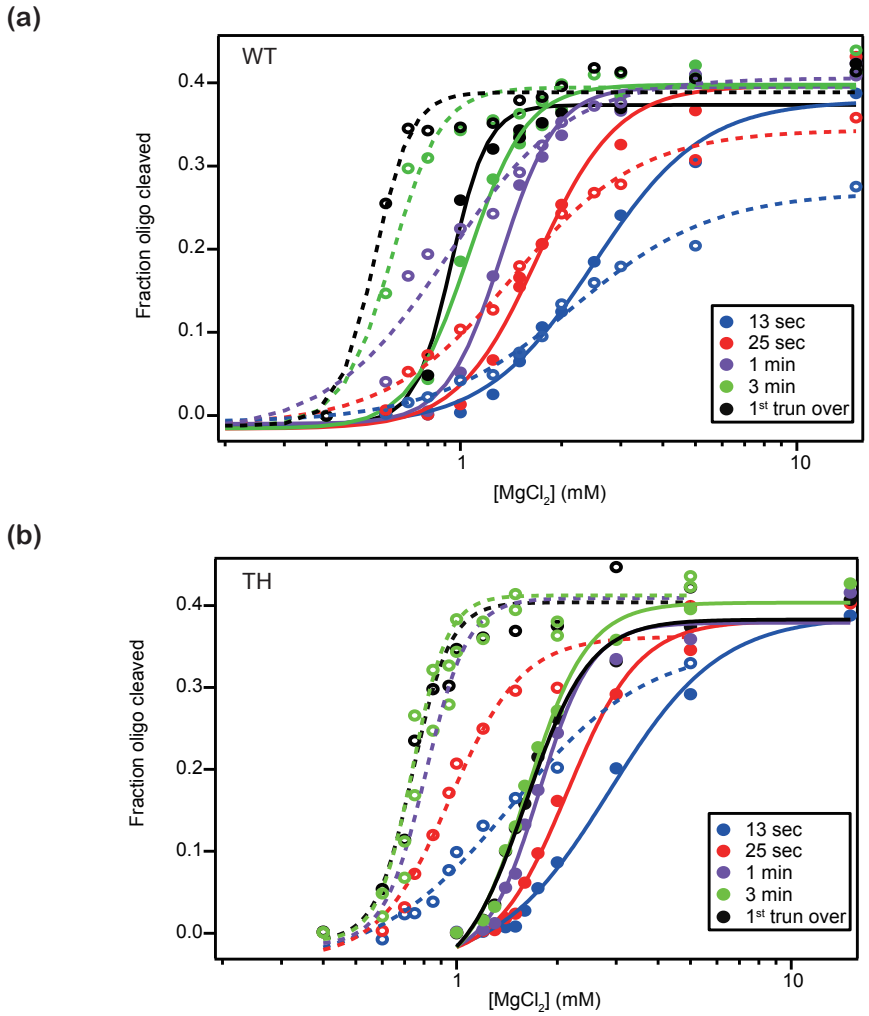

Figure S7. Cleaved product as a function of $MgCl_2$ concentration after different reaction intervals. Data from Fig. S4. (a) WT L-3 ribozyme; (b) TH L-3 ribozyme. The burst phase amplitudes (*A*) were obtained from fits to progress curves in Fig. S4 (black). Solid lines, no PEG; dashed lines, +18% PEG.

Figure S8

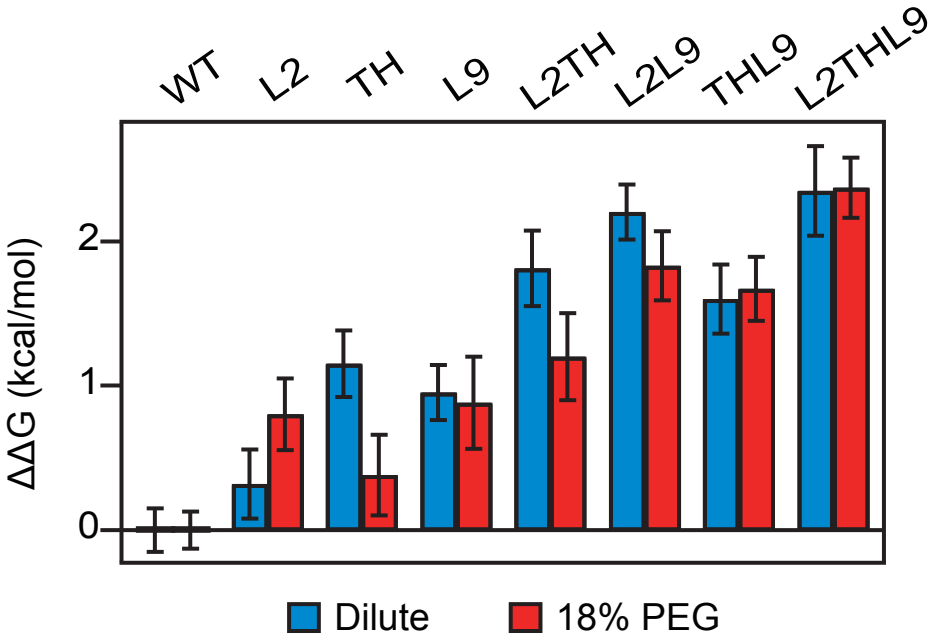

Figure S8. Folding free energies calculated from activity after 3 min. The folding free energies were evaluated at 0.88 mM $MgCl_2$ (dilute buffer), and 0.63 mM $MgCl_2$ (in 18% PEG) corresponding to 50% saturation of the respective WT folding transitions in each solution condition. Because the ribozyme is in large excess over substrate, these free energies reflect the total fraction of the RNA population able to access the reactive conformation at some point within the 3 min reaction time, rather than the fraction native RNA at any given moment. Error bars depict the standard deviation calculated from 10,000 resampling of fit residuals. The free energy obtained from activity assay is corrected for the relative maximum activity (Fig. S2).

Supplementary References

1. Rangan, P. and Woodson, S.A. (2003) Structural requirement for Mg2+ binding in the group I intron core. *J. Mol. Biol.*, **329**, 229-238.

2. Kilburn, D., Roh, J.H., Behrouzi, R., Briber, R.M. and Woodson, S.A. (2013) Crowders perturb the entropy of RNA energy landscapes to favor folding. *J. Am. Chem. Soc.*, **135**, 10055-10063.

3. Roh, J.H., Guo, L., Kilburn, J.D., Briber, R.M., Irving, T. and Woodson, S.A. (2010)

Multistage collapse of a bacterial ribozyme observed by time-resolved small-angle X-ray scattering. *J. Am. Chem. Soc.*, **132**, 10148-10154.

4. Woodson, S.A. and Koculi, E. (2009) Analysis of RNA Folding by Native Polyacrylamide Gel Electrophoresis. *Method Enzymol.*, **469**, 189-208.

5. Behrouzi, R., Roh, J.H., Kilburn, D., Briber, R.M. and Woodson, S.A. (2012) Cooperative tertiary interaction network guides RNA folding. *Cell*, **149**, 348-357.

6. Moghaddam, S., Caliskan, G., Chauhan, S., Hyeon, C., Briber, R.M., Thirumalai, D. and Woodson, S.A. (2009) Metal Ion Dependence of Cooperative Collapse Transitions in RNA. *J. Mol. Biol.*, **393**, 753-764.

7. Desai, R., Kilburn, D., Lee, H.-T. and Woodson, S.A. (2014) Increased ribozyme activity in crowded solutions. *J Biol Chem.*, **289**, 2972-2977.

8. Shi, X., Bisaria, N., Benz-Moy, T.L., Bonilla, S., Pavlichin, D.S. and Herschlag, D. (2014) Roles of long-range tertiary interactions in limiting dynamics of the Tetrahymena group I ribozyme. *J Am Chem Soc.*, **136**, 6643-6648.

9. Herschlag, D. and Cech, T.R. (1990) Catalysis of RNA cleavage by the Tetrahymena thermophila ribozyme. 1. Kinetic description of the reaction of an RNA substrate complementary to the active site. *Biochemistry*, **29**, 10159-10171.